PROCEEDINGS OF SPIE

SPIEDigitalLibrary.org/conference-proceedings-of-spie

3D photonic integrated 4x4 multi-mode interference coupler

Nuck, Madeleine, Kleinert, Moritz, Conradi, Hauke, de Felipe, David, Zawadazki, Crispin, et al.

Madeleine Nuck, Moritz Kleinert, Hauke Conradi, David de Felipe, Crispin Zawadazki, Anja Scheu, Martin Kresse, Walter Brinker, Norbert Keil, Martin Schell, "3D photonic integrated 4x4 multi-mode interference coupler," Proc. SPIE 10921, Integrated Optics: Devices, Materials, and Technologies XXIII, 109211C (4 March 2019); doi: 10.1117/12.2509776

SPIE.

Event: SPIE OPTO, 2019, San Francisco, California, United States

3D Photonic Integrated 4x4 Multi-Mode Interference Coupler

Madeleine Nuck*[a], Moritz Kleinert[a], Hauke Conradi[a], David de Felipe[a], Crispin Zawadzki[a], Anja Scheu[a], Martin Kresse[a] Walter Brinker[a], Norbert Keil[a], Martin Schell[a]

[a] Fraunhofer Heinrich Hertz Institute, Photonic Components Dept., Einsteinufer 37, 10587 Berlin, Germany

*madeleine.nuck@hhi.fraunhofer.de

ABSTRACT

3D photonic integration introduces a new degree of freedom in the design of photonic integrated circuits (PICs) compared to standard 2D-like structures. Novel applications such as large-scale optical switching matrices, e.g. for top-of-rack cross connect switches in data centers, benefit from the additional design flexibility due to their waveguide crossing-free architecture and compact footprint. In this work, a novel 3D 4x4 multi-mode interference coupler (MMI) based on HHI's polymer-based photonic integration platform PolyBoard is presented. The fabrication process of the PolyBoard platform allows for the realization of vertically stacked polymer waveguide layers. Cascading two of the presented 3D 4x4 MMIs will form the building block of future large-scale 3D switching matrices.

The 3D 4x4 MMI structure comprises two waveguide layers separated by a distance of 7.2 µm, with two input and two output waveguides in each layer, and a multimode interference (MMI) section in between. The vertical MMI section serves as the interconnection between the different waveguide layers and distributes the incoming light from each input waveguide across the four output ports of the 4x4 MMI. Design rules and fabrication methodology of these novel structures are presented in detail. Preliminary measurements demonstrate the proof-of-concept indicating an insertion loss below 9.3 dB, including fiber-chip coupling loss and the 6 dB intrinsic loss.

Keywords: 3D photonic integration, polymer waveguides, optical switching matrices, 3D multi-mode interference coupler

1. INTRODUCTION AND MOTIVATION

3D photonic integration opens up a new degree of freedom in the design of photonic chips. This enables their use in novel applications such as large-scale crossing-free optical switching matrices, switchable connections of multi-core fibers with single-mode outputs, and 3D optical phased arrays for LIDAR. The use of the third dimension in these multi-layer waveguide system allows for the crossing-free routing of multiple optical flows in a photonic integrated circuit (PIC) [1]. Such 3D PICs were successfully fabricated in HHI's PolyBoard platform [1] – [3] with resulting waveguide losses below 1 dB/cm for all five stacked waveguide layers [4]. Additionally, a low-loss vertical MMI coupler between two waveguide layers with a vertical centre-to-centre waveguide distance of 7.2 µm [5] was recently demonstrated. This allows for an interconnection of two waveguide layers with an on-chip loss below 1.2 dB [5]. Furthermore, the PolyBoard technology allows the fabrication of more complex 3D structures, like 3D 4x4 crossing-free optical switching matrices, shown in Figure 1 [1]. The building block of this structure are two cascaded 3D 4x4 MMIs (Figure 2). This is the first step towards large-scale crossing-free switching matrices.

1.1 Functionality of a 3D 4x4 switching matrix

The switching matrix in Figure 1 consist of two cascaded 3D 4x4 MMIs (Figure 1) to connect the four single-mode input waveguides with each single-mode output waveguide in the 3D space [1]. In Figure 1(a), the functionality of cascaded 3D 4x4 MMIs without phase shifters is shown. The light is guided from one excited input waveguide [see intensity inset, Figure 1(a)] to the first multi-mode section [1]. There the intensity is uniformly distributed to the four output waveguides in two waveguide layers as shown in the middle intensity inset in Figure 1(a). In the second multi-mode section the light from the four inputs interferes again and only one output waveguide is excited [third intensity inset, Figure 1(a)] [1]. Hence, the light in the passive structure is routed from a single-mode input waveguide to a single-mode output

Integrated Optics: Devices, Materials, and Technologies XXIII, edited by Sonia M. García-Blanco, Pavel Cheben,
Proc. of SPIE Vol. 10921, 109211C · © 2019 SPIE · CCC code: 0277-786X/19/$18 · doi: 10.1117/12.2509776

waveguide. In order to achieve the ability to connect each input waveguide with every output, an active part is necessary. This can be realized by means of thermo-optical phase shifters [1, 2, 6] in the four waveguides connecting the MMI sections, as presented in Figure 1. Figure 1(a) corresponds to the passive structure with relative phase shifts of $\phi_{ij}=0$. By switching the induced phase shifts between 0 and π, the interconnection between the input and output waveguides can be altered [1] and the same excited input can be connect with every output waveguide by changing the phase [1]. The switching modes for one exemplary excited input waveguide are shown in Figure 1(a) to (d).

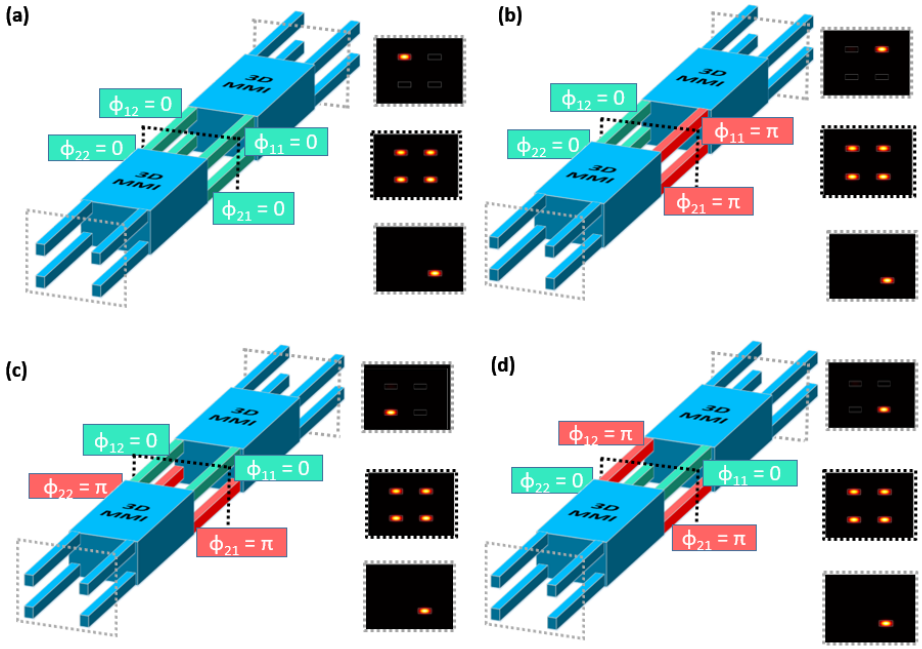

Figure 1: Concept of a 3D 4x4 crossing-free optical switching matrix in two waveguide layers based on two cascaded 3D 4x4 MMIs and thermo-optical phase shifters [1]. The four configurations (a) – (d) corresponds to the phase shifter settings: (a) $\phi_{11} = \phi_{12} = \phi_{21} = \phi_{22} = 0$; (b) $\phi_{11} = \phi_{21} = \pi$, $\phi_{12} = \phi_{22} = 0$; (c) $\phi_{11} = \phi_{12} = 0$, $\phi_{21} = \phi_{22} = \pi$ and (d) $\phi_{11} = \phi_{22} = 0$, $\phi_{12} = \phi_{21} = \pi$

The building block of a 3D 4x4 crossing-free optical switching matrix is the 3D 4x4 MMI structure and will be examined here in more detail. In this work, we present the design, fabrication and characterization of a polymer-based 3D 4x4 MMI in HHI's PolyBoard platform. The fabrication processes was optimized for the wafer-scale production of 3D structures [5]. This yielded in a functional 3D 4x4 MMI device.

2. DESIGN AND SIMULATION

The 3D 4x4 MMI design resembles two stacked planar 2x2 MMI panels with an interconnection between the layers. Figure 2 shows a 3D schematic of such a 3D 4x4 MMI. The structure consist of two input and two output single-mode waveguides per layer. The section between the waveguides is a 3D multi-mode interference region [1]. The refractive index of the polymer waveguide and cladding materials are 1.48 and 1.45, respectively. The waveguides have a cross section of 3.2 µm x 3.2 µm to ensure single-mode operation at a wavelength of 1550 nm. The design in Figure 2 shows five parameters: the height of the MMI section H_{MMI}; the length of the 3D MMI L_{MMI}; the width / depth of the 3D MMI W_{MMI}; the waveguide width w_{WG}, and the horizontal center-to-center waveguide distance on one layer out_D. The height of the 3D MMI is fixed at H_{MMI}=10.4 µm (vertical center-to-center distance 7.2 µm). In addition, the waveguide height is kept constant at 3.2 µm. The 3D 4x4 MMI comprises of three adjacent polymer layers (Figure 3) with heights of 3.2 µm, 4.0 µm, and 3.2 µm.

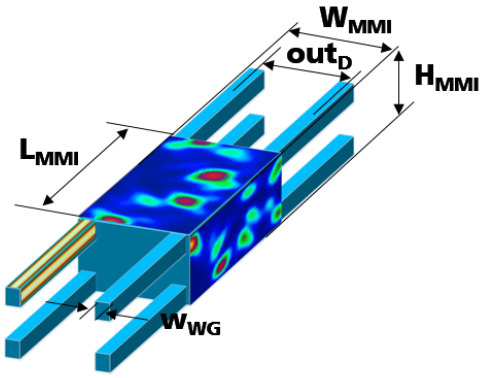

Figure 2: 3D sketch of a 3D 4x4 MMI with simulation results for the light intensity.

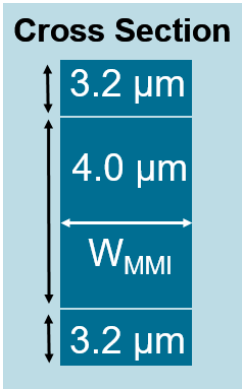

Figure 3: Schematic of the cross section of the 3D 4x4 MMI section with three waveguide layers.

2.1 Symmetries and nomenclature

The presented design has two planes of symmetry in the direction of light propagation, which are shown in Figure 4(a): a horizontal and a vertical plane through the middle of the structure. The horizontal plane connections of the input and output waveguides can be grouped into two categories: 'through' [Figure 4(b)] and 'cross' [Figure 4(c)]. By exploiting the vertical plane of symmetry, only one input waveguide per horizontal plane needs to be considered. From the symmetry follows that for the numerical optimization not all 16 interconnections must be studied, but only four. We call the interconnections 'through', if they keep their vertical position, and 'cross' otherwise. We add 'port 1' for an output waveguide of a horizontal layer, if they keep their horizontal position respective to the input waveguide, and 'port 2' otherwise. In addition, the input waveguides are numbered with I_j with j = 1, 2, 3, 4 [Figure 4(a)].

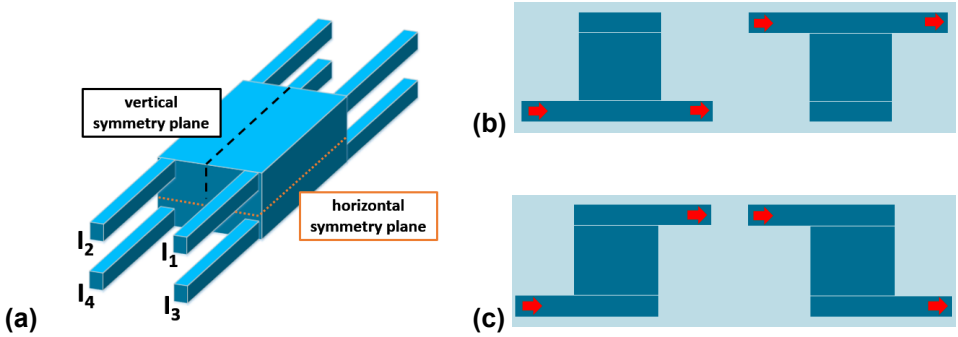

Figure 4: Sketch of the symmetry planes on a 3D 4x4 MMI. (a) Overview of a 3D 4x4 MMI with the horizontal and vertical symmetry plane. Grouped connection modes in (b) 'through' and (c) 'cross' shown in the longitudinal section of a 3D 4x4 MMI.

Taking into account the symmetry of the 3D 4x4 MMI, the four unknown parameters (L_{MMI}, W_{MMI}, w_{WG} and out_D) were determined in a numerical optimization step.

2.2 Numerical optimization of the design

The complete structure is implemented in FIMMWAVE. The four unknown parameters are optimized numerically at a wavelength of 1550 nm. The target is a design with low excess MMI losses (inclusive 6 dB intrinsic loss) and a minimal imbalance between the output waveguides. This yields a 3D structure with an equal distribution of the incoming light intensity across all outputs. The self-imaging theory of MMIs [7], [8] suggests that the length and width of the multi-mode area are correlated with each other.

This necessity specifies the following numerical optimization strategy. The 3D MMI width W_{MMI} is varied for different fixed lengths L_{MMI} at a waveguide width w_{WG} of 3.2 µm. The horizontal waveguide distance relates directly to the MMI width and changes simultaneously. For a length of 450 µm, the width is scanned in a range of 12 µm and 15 µm. Figure 5 shows a minimum MMI loss and a minimum imbalance between the outputs at a 3D MMI width of 13.5 µm. Furthermore, Figure 5 indicates that the imbalance does not drop to 0 dB at any width, but a residual imbalance of 2.4 µm remains.

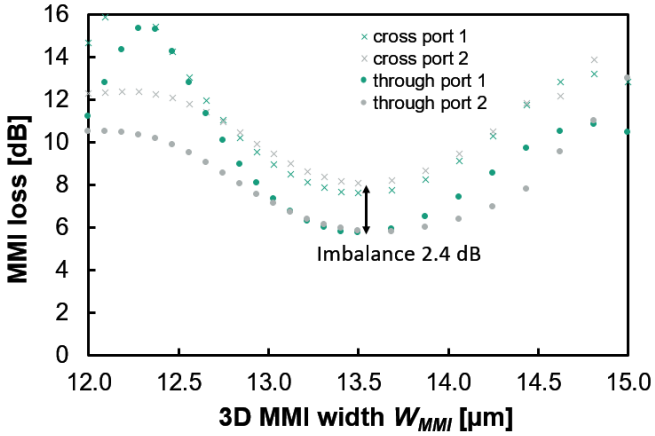

Figure 5: Simulated loss at 1550 nm as a function of the 3D 4x4 MMI width for a fixed 3D MMI length of 450 µm, a waveguide width of 3.2 µm. The horizontal waveguide distance changed with the 3D MMI width.

Similar to the previous procedure above the parameters w_{WG} and out_D were determined. The results of the respective parameter scan of the horizontal waveguide distance at a 3D MMI length of 450 µm and width of 13.5 µm are shown in Figure 6. For a waveguide width of w_{WG} = 3.5 µm, a horizontal waveguide distance of out_D = 9.6 µm (Figure 6) with low excess MMI losses of average 6.9 dB for the different connection modes and a minimum imbalance of 2.6 dB was found.

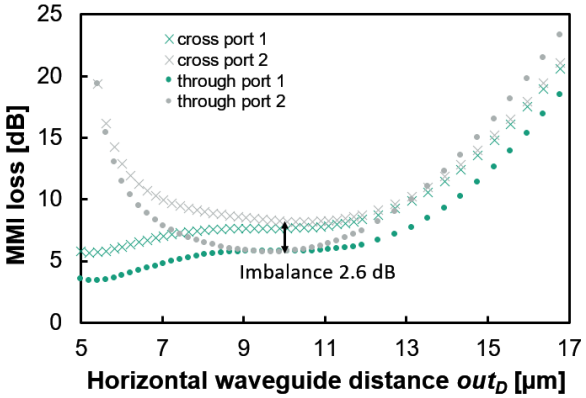

Figure 6: Simulated loss at 1550 nm as a function of the horizontal waveguide distance of a 3D 4x4 MMI for a fixed 3D MMI length of 450 µm, 3D MMI width of 13.5 µm and a waveguide width of 3.5 µm.

Again, the imbalance is not 0 dB in the optimum case (Figure 5 - Figure 6). A possible reason for this behavior is the fixed 3D MMI height of 10.4 µm. In a second iteration of the simulation, the length is varied for the previously optimized MMI width, waveguide width and horizontal waveguide distance. In Figure 7 the MMI loss as a function of the 3D MMI length is shown. It exhibits a minimum average loss at a length of 447 µm. In Figure 8 the imbalance is presented for the same length range from 400 µm up to 500 µm. The point of minimal imbalance (0.3 dB) at a length of 476 µm does not corresponds to the point of minimal excess loss for the 3D 4x4 MMI.

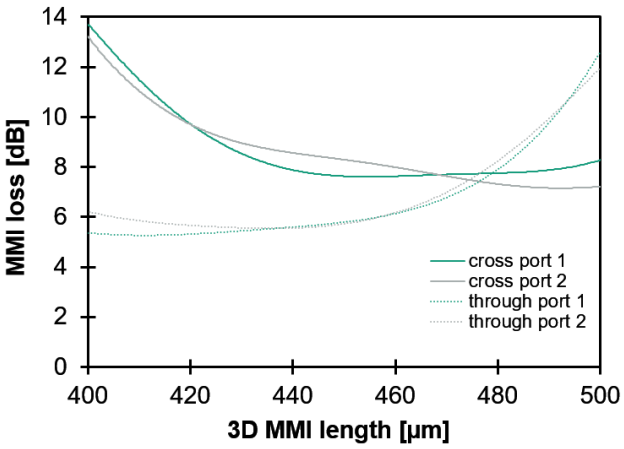

Figure 7: Simulated loss at 1550 nm as a function of the 3D MMI length for a fixed 3D MMI width of 13.5 µm, waveguide width of 3.5 µm and horizontal waveguide distance of 9.6 µm.

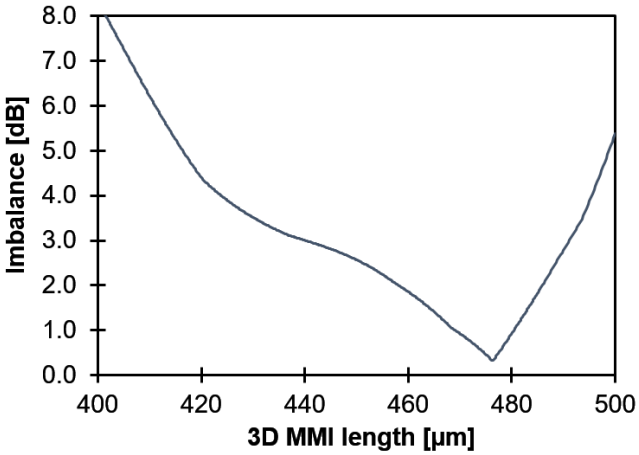

Figure 8: Simulated imbalance at 1550 nm as a function of the 3D MMI length for a fixed 3D MMI width of 13.5 µm, waveguide width of 3.5 µm and horizontal waveguide distance of 9.6 µm.

3. TECHNOLOGY AND FABRICATION PROCESS

The following section introduces the fabrication process of 3D MMIs in the PolyBoard platform and compares the standard fabrication process [9] with an optimized process. The waveguide and cladding layers consist of polymer material of the ZPU-12 series from ChemOptics Inc. [10]. The standard fabrication process is shown in Figure 9(a). The 3D structure consist of three waveguide layers (Figure 3), which are in direct contact [9]. The first two steps in Figure 9(a) are identical to the fabrication of a standard planar waveguide structure. The liquid polymer resin (waveguide / cladding) is spin-coated on a wafer and subsequently cured by UV exposure and baking. The waveguide layer is structured by UV lithography and deposition of a titanium hard mask (Ti-mask) for the subsequent structuring with oxygen plasma reactive ion etching (RIE). After that, a second cladding layer is spin-coated on top [Figure 9(a)].

For the 3D structure, the waveguide layers have to be in a direct contact with the adjacent waveguide layers. This was identified to be the most critical point during the fabrication process. The cladding material on top of the top side of the ground waveguide is thinned using RIE. In this thinning step (Figure 9) the ground waveguide is also partially etched. This sequence is repeated for the middle and top waveguide layers. The final layer sequence of the 3D MMI is shown in Figure 3.

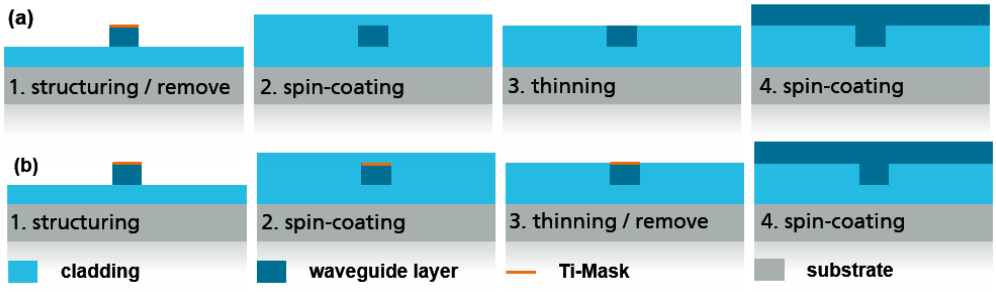

Figure 9: Schematic sketches of the fabrication process sequence of a 3D MMI for the standard process (a) [9] and the optimized process (b) [5].

The standard process was optimized in the critical thinning step by adapting the step sequence. In the optimized process in Figure 9(b), the Ti-mask is left in place on top of the waveguide until the end of the thinning step [5]. This approach has two advantages: On one hand, the Ti-mask protects the ground waveguide structure against the etching by RIE. On

the other hand, this approach allows for a more precise control of the layer thickness and the etching process of the cladding layer on top of the ground waveguide. After reaching the top edge of the ground waveguide, the Ti-mask is removed. The three steps up to the thinning/remove step in Figure 9(b) are repeated for the middle and top layer waveguide. In the end, the layer sequence is similar to the standard process (Figure 3).

This optimized process was used for the fabrication of 3D 4x4 MMIs on 4-inch-wafer scale.

4. CHARACTERIZATION

Optical transmission measurement were conducted on the fabricated 3D 4x4 MMI. The wavelength-dependent on-chip loss through and cross a 3D 4x4 MMI for one input waveguide (I_1), is shown in Figure 10. The measurement demonstrate that the light intensity from the input I_1 is indeed distributed across all four output waveguides. Additionally to the measured curve, the simulation results for a fixed parameter combination (L_{MMI}=470 µm, W_{MMI}=13.5 µm, w_{WG}=3.5 µm, out_D=9.0 µm) are shown in Figure 10. The comparison shows that the curves (measurement and simulation) for the connection mode cross port 2 are close together. The measured curve cross port 2 has a minimum on-chip loss at 1553 nm. Furthermore, the measured spectrum of cross port 1 are close to the simulation curve at 1540 nm (Figure 10). Noticeable are the higher difference between measurement and simulation for the connection mode through port 1 / 2. This leads to an imbalance of more than 2 dB at 1550 nm. The reason for these deviations could be an unintended change of the geometrical device parameters (L_{MMI}, W_{MMI}, w_{WG}, out_D) during the optimized fabrication process.

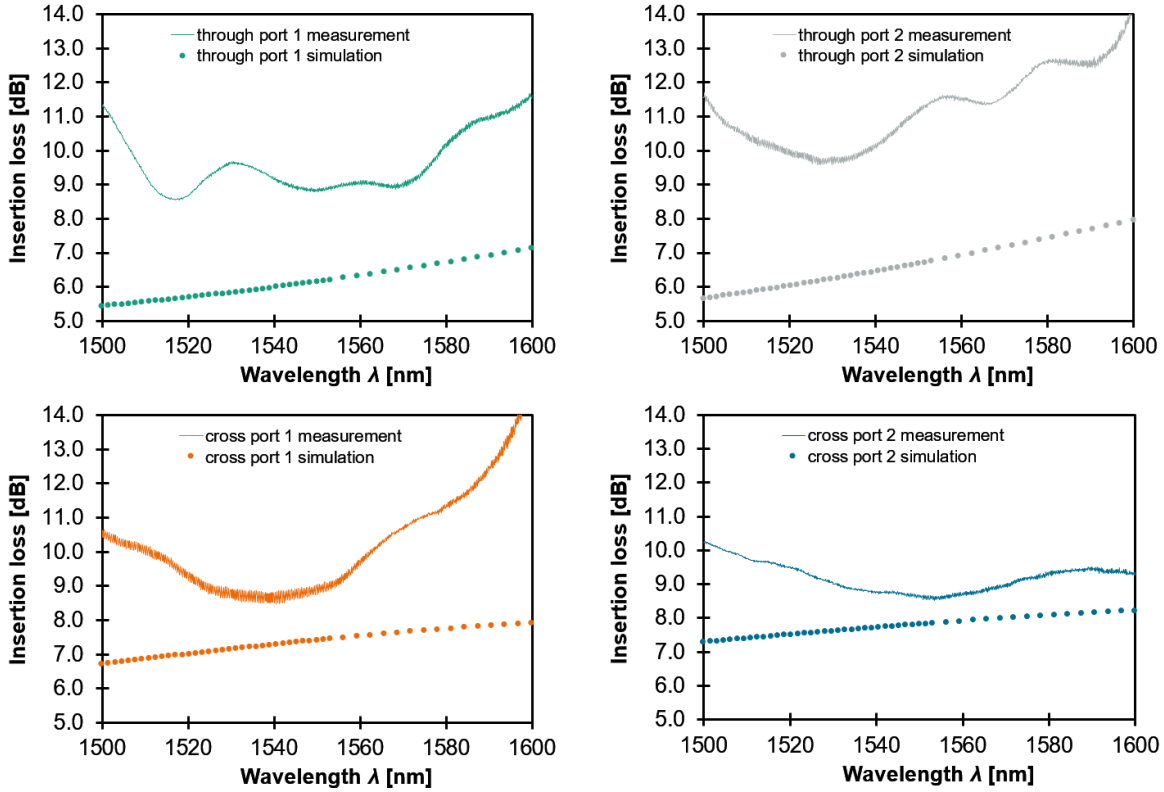

Figure 10: Optical transmission measurements on a 3D 4x4 MMI for one input I1 with all connection modes for a 3D MMI length of 470 µm, width of 13.5 µm, waveguide width of 3.5 µm and a horizontal waveguide distance of 9.0 µm (includes 1.2 dB: material absorption, fiber-chip-fiber coupling loss; loss determined with straight reference waveguides). Additionally, for each connection the simulation results for the given parameters are shown.

Figure 11 shows the on-chip losses for all interconnections of the same structure at a fixed wavelength of 1550 nm. It can be seen that all 16 connections are working. For three of the four input waveguides, the connection mode through port 2 has the highest insertion losses. This does not correspond to the behavior expected from the simulation values in Figure

11. The observed behavior suggests that the high insertion losses in connection mode through port 2 are not specific to the horizontal waveguide layer and hence not caused by increased losses in a single waveguide layer. Therefore, it can be reasoned that the high losses and imbalance (> 5 dB) between the output waveguides is caused by the deviation of a higher-level structure parameter, such as the 3D MMI width or the effective refractive indices, form the assumptions of the simulations.

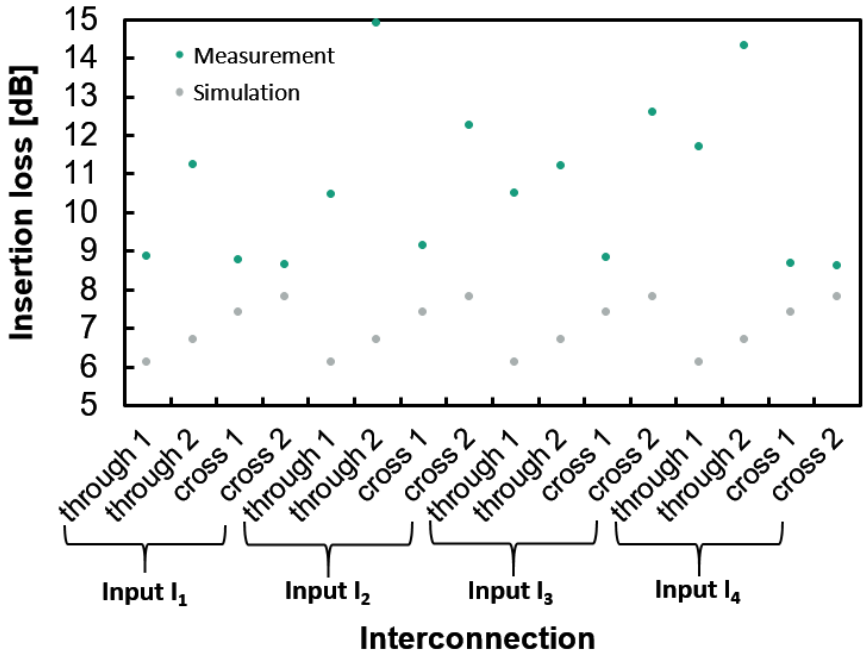

Figure 11: Measured and simulated insertion losses for each interconnection of a 3D 4x4 MMI (length of 470 µm, width of 13.5 µm, waveguide width of 3.5 µm, horizontal waveguide distance of 9.0 µm and includes 1.2 dB: material absorption, fiber-chip-fiber coupling loss; loss determined with straight reference waveguides) at a wavelength of 1550 nm.

As mentioned, the crucial parameter for the high losses and high values of the imbalance could be the width of the 3D MMI. For a more detailed inversitgation, 3D 4x4 MMIs with varying MMI length L_{MMI} in a range of 400 µm up to 500 µm were examined. Figure 12 shows the measurement results of the imbalance for each device as a function of the 3D MMI length for a fixed width of 13.5 µm at a wavelength of 1550 nm. The measured imbalance has a minimum of 5.6 dB at 465 nm. Furthermore, Figure 12 shows the simulation values for the length variation 3D MMIs with two different widths W_{MMI}=13.5 µm (red line) and W_{MMI}=11 µm (green line). The measurement deviates by 5 dB from the simulation curve of the nominal width of 13.5 µm. On the other hand, the green simulation curve for a smaller 3D MMI width of 11 µm is close to the measured curve with a difference of the imbalance of 0.6 dB. Hence, it can be assumed that the effective width of the fabricated structures is smaller than expected by 2.5 µm. According to the self-imaging theory [7, 8] of MMIs, this leads to a shift of the optimum MMI length towards smaller values. This results in a higher imbalance between the output waveguides for the considered length range between 400 µm and 500 µm. Smaller effective widths of the 3D 4x4 MMIs can be resulted from two points in the fabrication process. On the one hand, during the structuring step (Figure 9) with RIE, the vertical sidewalls are also slightly etched and the width of the respective waveguide section is reduced. As a reduction is to be expected for each waveguide layer, resulting in a narrower effective width. Additionally, there can be a longitudinal shift between the three waveguide layers. This leads to a smaller overlapping area of the MMI section and reduces the effective width of the device. On the other hand, the effective refractive indices in the structure can be deviation than expected in the simulation. One reason for this may be the interfaces in the multiple waveguide layer system.

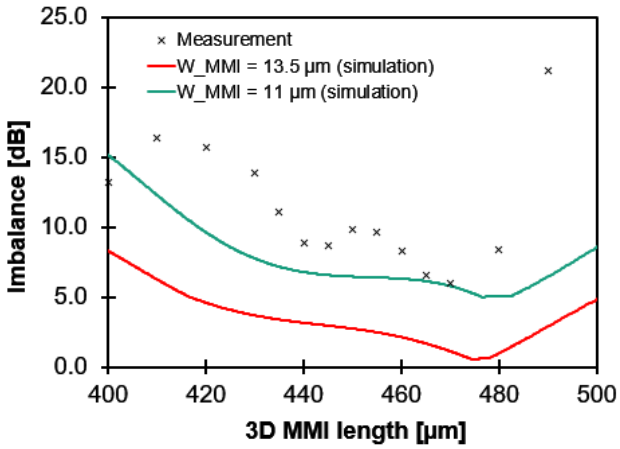

Figure 12: Imbalance as a function of the 3D MMI length for measurement (crosses) and simulation (red and green line) for a waveguide width of 3.5 µm and horizontal waveguide distance of 9.0 µm. The measurement results are obtained from structures with a nominal 3D MMI width of 13.5 µm.

While there is still a lot of room for improvement in insertion loss and imbalance, a proof-of-concept with working connections between all input and output waveguides of a 3D 4x4 MMI is realized, and the wafer-scale fabrication of a 3D MMI structure has been successfully implemented.

5. CONCLUSION

A 3D 4x4 MMI was designed and successfully fabricated with an optimized fabrication process in the PolyBoard hybrid photonic integration platform. Optical transmission measurements show that the connection of every input with every output waveguide is possible. In a new iteration of the fabrication process, the design can be adjusted in terms of the 3D MMI width to obtain the optimized width of 13.5 µm in the fabricated devices. This work paves the way towards the development of novel applications for 3D photonic integrated circuits. In a next step, a device with two cascaded 3D 4x4 MMIs will be fabricated, resulting in a 3D 4x4 switching element. This building block enables new applications like 3D optical phased arrays for LIDAR and switchable interconnections for multi-core fibers to classical planar PICs.

ACKNOWLEDGEMENTS

This work was partially funded by the European Commission through the project ICT-3PEAT [contract number 780502] and partially funded by European Regional Development Fund (ERDF) and Berlin thought the project “Leistungszentrum Digitale Vernetzung”.

REFERENCES

[1] D. de Felipe et al., “Recent Developments in Polymer-Based Photonic Components for Disruptive Capacity Upgrade in Data Centers,” J. of Lightwave Technology, Vol. 35, no. 4, p. 683 (2017).
[2] M. Kleinert et al., “Photonic integrated devices and functions on hybrid polymer platform,” Photonics West, 10098-45 (2017).
[3] D. de Felipe et al., “Recent Developments in the Polymer Photonic Integration Technology,” IPR 2016, Vancouver (2016).
[4] Z. Zhang et al., “Multicore polymer waveguides and multistep 45° mirrors for 3D photonic integration,” IEEE Photon. Technol. Letter, Vol. 26, no. 19, p. 1986 (2014).
[5] M. Nuck et al., “Low-loss Vertical MMI Coupler for 3D Photonic Integration,” ECOC, Tu3.C4 (2018).
[6] A. Maese-Novo et al., “Thermally optimized variable optical attenuators on a polymer platform,” Applied Optics, Vol. 54, no. 3, p. 569 (2015).

[7] L.B. Soldano et al., „Optical Multi-Mode Interference Devices Based on Self-Imaging: Principles and Applications," J. of Lightwave Technology, Vol. 13, no. 4, p. 615 (1995).
[8] J. Zhao et al., "Optimal design of multimode interference couplers using an improved self-imaging theory," Optics Communications, Vol. 281, p. 1576 (2008).
[9] J.-M. Lee et al., "Vertical Coupling of Polymeric Double-Layered Waveguides Using a Stepped MMI Coupler," ETRI Journal, Vol. 25, no. 2, p. 81 (2003).
[10] ChemOptics Inc., http://www.chemoptics.co.kr (2018).